Limnol. Oceanogr., 58(2), 2013, 579–592

doi:10.4319/lo.2013.58.2.0579

Mixing of an interflow into the ambient water of Lake Iseo

Charlie A. R. Hogg,[a,*] Clelia L. Marti,[b] Herbert E. Huppert,[a,c] and Jörg Imberger [b]

[a] Institute of Theoretical Geophysics, Department of Applied Mathematics and Theoretical Physics, University of Cambridge, Cambridge, United Kingdom

[b] Centre for Water Research, University of Western Australia, Crawley, Western Australia, Australia

[c] School of Mathematics, University of New South Wales, Sydney, New South Wales, Australia

Abstract

River water flowing as an interflow was investigated using field data, collected in Lake Iseo (Italy), and theory. A theory for the lateral falling mechanism of plunging was developed for inflows when the initial densimetric Froude number (Fr_0) is slightly larger than unity. The ratio of the river width to the offshore extent of the plunge region was equal to Fr_0. The mixing ratio in the plunge region was 0.06. Theoretical results were quantitatively consistent with the length scale and mixing ratio of the observed plunge region. The progression of the inflow was interpreted as: initially a laterally falling plunge region with little mixing; followed by a steep underflow region with substantial mixing; and finally an intrusion. The intrusion was at first controlled dynamically by an inertia-buoyancy force balance. Further from the liftoff point, turbulent mixing effects dominated over those due to inertia. Ultimately, the intrusion diffused into the adjacent layers in such a way that the interflow fluid was effectively indistinguishable from the lake water.

The passage of water from a river inlet to an intrusion can be the dominant driver of ecology within a lake, yet current quantitative understanding of this transport is not satisfactory (Rueda et al. 2007). The motion of water entering a lake from a river can take various forms depending on the density of the inflow water relative to the density of the receiving lake surface water (Serruya 1974). Inflowing water less dense than the lake surface water will flow along the surface of the lake as an overflow (Chen 1980; Luketina and Imberger 1987; Cáceres et al. 2002). Inflowing water denser than the surface water of the lake will descend along the lake bed to enter at a level of neutral buoyancy as an interflow (Imberger and Patterson 1989). If the inflow never becomes neutrally buoyant, the inflow will enter at the bottom of the lake as an underflow (Hebbert et al. 1979).

The nutrient loading to a lake normally comes from river inflows, so the ecological response of the lake is very sensitive to changes in the inflow behavior (Rueda and MacIntyre 2009; Vilhena et al. 2010; Marti et al. 2011). Incorrect modeling of the dilution of an inflow can give rise to errors in both the intrusion depth and the availability of nutrients to the primary producers in the surface layer (Rueda et al. 2007). In addition, the public health risk posed by pathogens that enter with the river depends on the dilution and horizontal extent of the inflow (Antenucci et al. 2005). Knowledge of the behavior of river inflows is still not complete. The primary deficiencies addressed in this paper are the dynamics of inflows in three-dimensional (3D) inlet geometries and the amount of dilution in the plunge region.

General reviews of inflows include those by Ford and Johnson (1983), Imberger and Patterson (1989), and Alavian et al. (1992). The consecutive stages along an inflow are governed by different dynamics. We consider here the three dynamical regimes of an interflow in turn: (1) the plunge stage, (2) the underflow stage, and (3) the intrusion stage. These stages are shown schematically in Fig. 1.

Plunge stage—When a relatively dense river flows into a lake, the river water flows as a uniform layer until the water reaches the plunge region. Four distinct, although not exhaustive, cases may be defined, depending upon the geometry and dynamics of the river.

(1) A two-dimensional (2D) plunge point occurs when the dynamic pressure of the inflowing river water, $\rho_r u_0^2/2$, becomes less than the hydrostatic pressure difference, $\rho_r g'_0 H$, where ρ_r is the reference density, u_0 the velocity of the water, $g'_0 = g\Delta\rho/\rho_r$ the reduced gravity of the river water with respect to the lake surface water, g the acceleration due to gravity, $\Delta\rho$ the difference in density between the river water and the lake surface water, and H the depth of the water column at the plunge region. This transition implies that the densimetric Froude number ($Fr = u_0/\sqrt{g'_0 H}$) is of order unity. As the inflow is no longer able to push back the lake water, the inflow plunges beneath the surface with an initial underflow depth of half the channel depth (Benjamin 1968).

(2) The case of a drowned river valley characterized by a sloping channel with a triangular cross section was originally described and observed in the field by Hebbert et al. (1979). The triangular cross section alters the vertical distribution of the force due to hydrostatic pressure. The slope causes the water depth to increase and the dynamic pressure to reduce along the river. At a critical depth, the dynamic pressure becomes less than the hydrostatic pressure difference and plunging occurs.

* Corresponding author: chogg@cantab.net

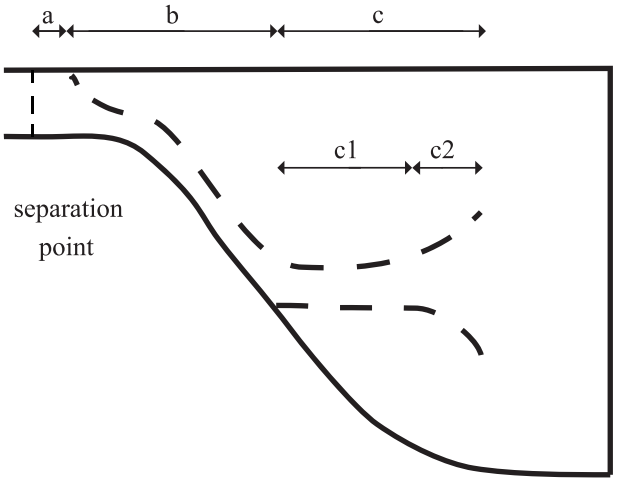

Fig. 1. Schematic showing length scales of the consecutive stages of an interflow: (a) the plunging stage, (b) the underflow stage, (c1) the inertia-buoyancy intrusion stage, and (c2) the diffusion-buoyancy intrusion stage.

(3) Johnson et al. (1987) examined plunge regions formed when a river with a horizontal riverbed suddenly widens and separates as it enters a lake, as shown in plan form in Fig. 2. They only considered the scenario where lateral turbulent mixing dominates gravitational slumping. The inflowing river water forms a 3D plunge region. When the relative density difference between the river water and receiving water is small at the inlet (i.e., $Fr_0 \gg 1$), the mechanism for plunging is that the inflow forms a turbulent jet that entrains lake water horizontally inward across the shear layers on either side of the inflow. The entrainment decreases Fr to the critical value, $Fr_C \sim 1$, at which point the inflow plunges. The model for the evolution of Fr along the jet is derived from conservation of volume, momentum, and buoyancy, and an entrainment law that the jet's volume flow scales with the square root of the distance offshore (Fischer et al. 1979). The jet reaches the critical value of Fr at the offshore extent of the plunge region, given by

$$x_j = 0.52 W Fr_0^4 \tag{1}$$

where W is the width of the channel and Fr_0 is the Froude number at the separation point (Morton et al. 1956; Stefan and Johnson 1989).
The mixing ratio in the plunge region, $\gamma_p = (Q_p - Q_0)/Q_0$, derived from the same entrainment model, is given by

$$\gamma_p = 0.5\left(x_j/W\right)^{1/2} - 1 \tag{2}$$

where Q_0 is the initial volume flow rate of the inflow and Q_p the flow rate after the plunge (Johnson et al. 1989). The laboratory evidence of Johnson et al. (1989) supports this model in the parameter range $1 < \gamma_p < 3$, although their conclusions are based on only three data points.

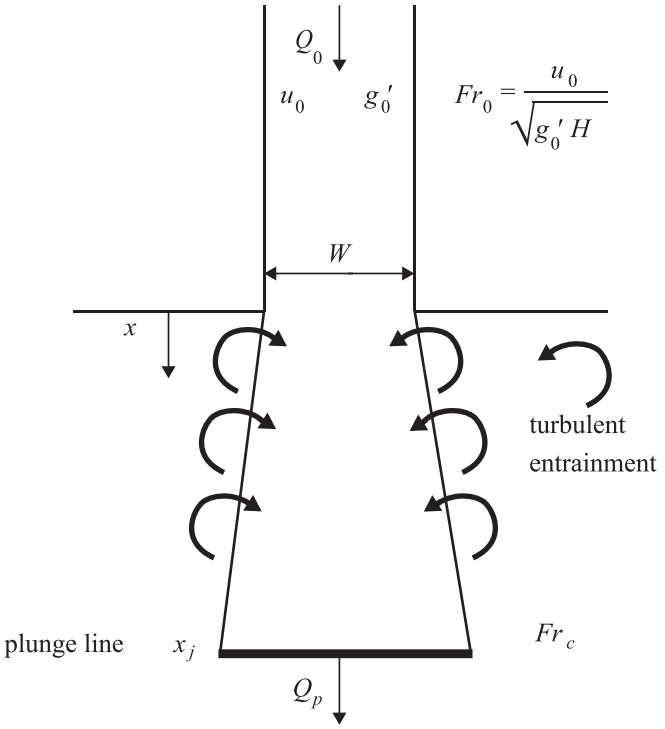

Fig. 2. Plan view, from above, of a river entering a lake as an entraining jet, showing our interpretation of the analysis of Johnson et al. (1987).

(4) When the river directly enters the lake, as in the third case, but the relative density differential between the river water and the receiving water is large and the inflow velocities are small (i.e., Fr_0 is only slightly larger than unity), the separated jet will slump laterally. When this occurs, the vertical stratification suppresses mixing and the entering fluid spreads laterally as it flows into the receiving water. This case was observed in Lake Iseo, and a theory describing it is presented below.

In field experiments in reservoirs in the Tennessee River basin, Elder and Wunderlich (1972) measured the combined entrainment in the plunge region and underflow, but did not isolate the separate contributions. The ratio of entrained water volume to initial water volume ranged from 0.02 up to 0.46. Fleenor (2001) carried out tracer dilution tests in the Whiskeytown River valley (in California), which had sharply diverging and converging riverbanks, and reported γ_p ranging from 0.2 to 0.7. For channels for which the half angle formed by the diverging channel walls is $> 7^\circ$, a linear regression of his field results and the laboratory results of Johnson et al. (1989) gave:

$$\gamma_p = 0.223 Fr_0 + 0.008\alpha \tag{3}$$

where α is the divergence half angle formed by the channel walls, measured in degrees, at the separation point of the

river (Fleenor 2001). Spigel et al. (2005) measured γ_p for two inflows into Lake Taupo (New Zealand) using a tracer injection method and found that γ_p was 1.87 and 1.94 in the two inflows, respectively. To find a linear relationship between γ_p and Fr_0, different site-specific coefficients were required for each inflow. These studies show that there are large variations in plunge region mixing.

Underflow stage—After the plunge region, a dense underflow will run along the lake bed to the depth of neutral buoyancy (Hebbert et al. 1979). If the bed slope varies only gradually, the bulk Richardson number quickly reaches a value that remains constant along the slope, a condition that is known as normal flow (Ellison and Turner 1959) and is dynamically analogous to uniform open channel flow. The bulk Richardson number is defined as $Ri = g'_u h/U^2$, where g'_u is the reduced gravity of the underflow, h is the thickness of the underflow, and U is the speed of the current along the slope. When normal flow theory is applied to the case of a triangular cross-sectional channel with a uniform density ambient, the evolution of the volume flow rate of the underflow along the slope, Q_u, is given by:

$$Q_u = Q_0[6Es/(5h_0) + 1]^{5/3} \tag{4}$$

where h_0 is the initial thickness of the underflow, Q_0 the underflow's initial volume flow rate, and s the distance along the lake bed (Hebbert et al. 1979). The entrainment constant is $E = U/W$, where W is the entrainment velocity perpendicular to the slope. To calculate the evolution of an underflow where the ambient water is stratified, Antenucci et al. (2005) showed that Eq. 4 could be applied locally, which is again analogous to gradually varied open channel flow.

Entrainment into the underflow requires that turbulent kinetic energy (TKE) is converted into gravitational potential energy in order to mix the overlying lighter water into the underflow (Sherman et al. 1978). The TKE may be generated either from stirring by the bottom roughness beneath the underflow or, at lower bulk Richardson numbers, from shear production at the upper interface of the underflow (Dallimore et al. 2001; Fernandez and Imberger 2006). A parameterization of the entrainment that is valid in both the stirring or shear production regimes has been used to provide E in Eq. 4 (Sherman et al. 1978).

Dallimore et al. (2004) coupled the underflow model described in Sherman et al. (1978) with the 3D lake hydrodynamic Estuary Lake and Coastal Ocean Model (ELCOM) (Hodges et al. 2000) and compared model results to field observations. The free surface height of the lake model was used to set the plunge location and to limit the depth of the underflow in the plunge region. The underflow was modeled by applying the vertically integrated conservation equations to the underflow. The model assumed that no mixing occurred within the plunge region. The absence of a parameterization for mixing within the plunge region was highlighted as a remaining limitation in this and other inflow models (Rueda and MacIntyre 2009).

Intrusion stage—At the depth of neutral buoyancy, the underflow stops descending, separates from the lake bed, and intrudes into the ambient lake water at the isopycnal depth (Imberger 1985). The intrusion is governed at first by an inertia-buoyancy force balance that extends to where inertia, buoyancy, and vertical diffusion all balance (Imberger 1972). For inflow regions with a half-width smaller than the length scale of the inertia-buoyancy intrusion, the flow may be modeled as 2D. The length scale of the inertia-buoyancy intrusion is given by:

$$x_i = q^{3/2} N^{-1/2} \kappa^{-1} \tag{5}$$

where q is the source volume flow per unit width, N the buoyancy frequency of the ambient (assumed locally constant), and κ the vertical turbulent diffusivity (Imberger et al. 1976). The turbulent diffusivity represents an average of all the distinct mixing events occurring at the intrusion. In the inertia-buoyancy intrusion, the velocity has been shown in laboratory experiments and theory to be given by:

$$u_i = N\delta_i \tag{6}$$

and the intrusion thickness to be constant and given by (Manins 1976):

$$\delta_i = (q/N)^{1/2} \tag{7}$$

A 2D intrusion in the diffusive-buoyancy regime moves with velocity:

$$u_v = Ax^{-1/3} \tag{8}$$

and has thickness:

$$\delta_v = \beta(x\kappa/N)^{1/3} \tag{9}$$

where β is an empirical constant with a value of 7.1 and x is the distance from the source (Koh 1966). The position of a parcel of fluid is

$$x = [4(At + B)/3]^{3/4} \tag{10}$$

where t is the time that the parcel has been in the diffusive-buoyancy regime, and both A and B are boundary parameters. The distance to the virtual origin x_v for the diffusive-buoyancy regime may be found from Eq. 9 by matching the thickness of the two intrusion regimes. The distance from the virtual origin to the start of the diffusive-buoyancy regime, when $t = 0$ in Eq. 10, yields the boundary parameter $B = 3x_v^{4/3}/4$. Additionally, continuity allows the velocity of the diffusive-buoyancy intrusion, given by Eq. 8, to be matched to the velocity of the inertia-buoyancy intrusion, to yield the boundary parameter $A = u_i x_v^{1/3}$. As the intrusion advances in the diffusive-buoyancy stage, the intrusion diffuses into the adjacent layers of ambient water. The diffusion occurs over a characteristic time scale $t_d \sim \delta_v^2/\kappa$. The characteristic length scale over which the intrusion diffuses into the background fluid is therefore given by:

$$x_d \sim \left[4/(3\beta) + 1/\beta^4\right]^{3/4} q^{3/2} N^{-1/2} \kappa^{-1} \tag{11}$$

In this study, the influence of rotation has not been considered. The Rossby number in the plunge region and

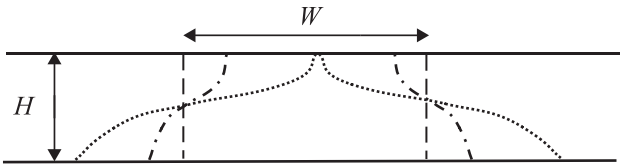

Fig. 3. Three transverse sections of the plunge region showing the progression of the lateral falling mechanism. The plunge region begins at the point of separation from the riverbanks where the inflow has the shape of the river channel (dashed). Within the plunge region, the edges of the inflow fall laterally (dot-dashed), until the entire inflow falls below the surface (dotted).

underflow is typically too large for rotation to influence the dynamics.

The main contribution of this paper is to present field measurements of the length scales and mixing ratios in the three consecutive stages of an interflow. The measurements are then compared with the existing models of the dynamics of interflows. A novel model of the plunge region, not to our knowledge previously discussed in the literature, is presented and compared with field measurements. The rest of the paper is structured as follows. The first section develops a theory for plunge regions in the regime of Fr_0 slightly larger than unity. The second section describes the field campaign. The third section provides calculations of the observed length scales and mixing ratios in the interflow. The final section highlights the significance of our findings when analyzing inflow behavior.

Theory

The derivations of x_j and γ_p in Eqs. 1 and 2 assume that an entrainment law can be applied to the inflow. At Fr_0 slightly larger than unity, however, buoyancy dominates before lateral entrainment can affect the inflow. Thus, because the stratification suppresses the turbulence, the entrainment law (Johnson et al. 1989) used in turbulent jet theory is not applicable. Furthermore, because at Fr_0 slightly larger than unity the plunge region does not extend into the zone of established flow, which begins at a distance $O(W)$ from the inlet, the assumed entrainment law is not applicable (Fischer et al. 1979). The mechanism applicable for the range of Fr_0 slightly larger than unity is that baroclinic generation of vorticity causes the inflow to fall away laterally such that the inflow water eventually plunges entirely below the lake surface. The progression of this falling motion is shown, schematically, in Fig. 3. This is similar to the mechanism proposed for buoyant surface trapped plumes (Chen 1980).

To analyze this lateral falling motion, consider a box model of a transverse slice of river water entering the lake. When the river water separates from the riverbanks, the river water has lighter lake surface water on either side. The different densities of the horizontally adjacent water bodies give rise to lateral baroclinic forces that accelerate the river water downwards and laterally outwards. The lateral motion is similar to the initial slumping phase of a gravity current after a lock release (Huppert and Simpson 1980).

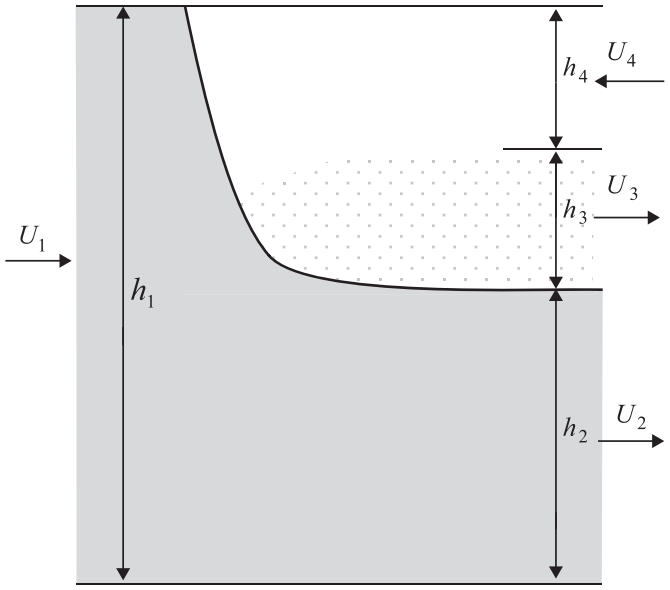

Fig. 4. Laboratory configuration to measure entrainment into a gravity current held stationary by an opposing flow. This is also the configuration of the surface lake water held stationary at the plunge region. The surface lake water mixes with the underflow and leaves the plunge region in layer 3.

As the river spreads laterally along the lake bed, water from either side of the inflow travels along the surface of the lake towards the midpoint of the river at speed $u_r = \sqrt{g'_0 H}/2$ (Shin et al. 2004). On the surface of the lake, the curve that separates the river water from the lake water is defined as the plunge curve. The point on the surface at which the lake water from both sides meets and the river water is fully submerged defines the offshore extent of the plunge region, x_g. The ratio x_g/W is identical to the ratio of the lateral to axial velocity, where the axial velocity is assumed to remain constant at u_0. This analysis gives:

$$x_g = u_0 W / \sqrt{g'_0 H} \tag{12}$$

When Fr_0 is only slightly larger than unity, entrainment is primarily caused by shear between the falling river water and the overlying stationary lake surface water. Entrainment at such a front was measured in gravity current laboratory experiments used to investigate entrainment into sea breeze fronts (Britter and Simpson 1978). A saline gravity current was held stationary in a steady state by fluid flowing against the flow of the gravity current, as shown in Fig. 4. The current was in a 2D channel of constant depth. The experiments measured the volume entrained across the shear interface into the opposing flow. The experimental results of Britter and Simpson (1978) may be applied to the mixing of lake surface water into the inflow in the plunge region. Downstream of the plunge region, the mixed fluid (layer 3 in Fig. 4) falls below the lake surface water to become mixed with the underflow. The experimental results yield:

$$\gamma_p = k/4 = 0.06 \tag{13}$$

where k is a universal empirical constant experimentally evaluated as 0.22.

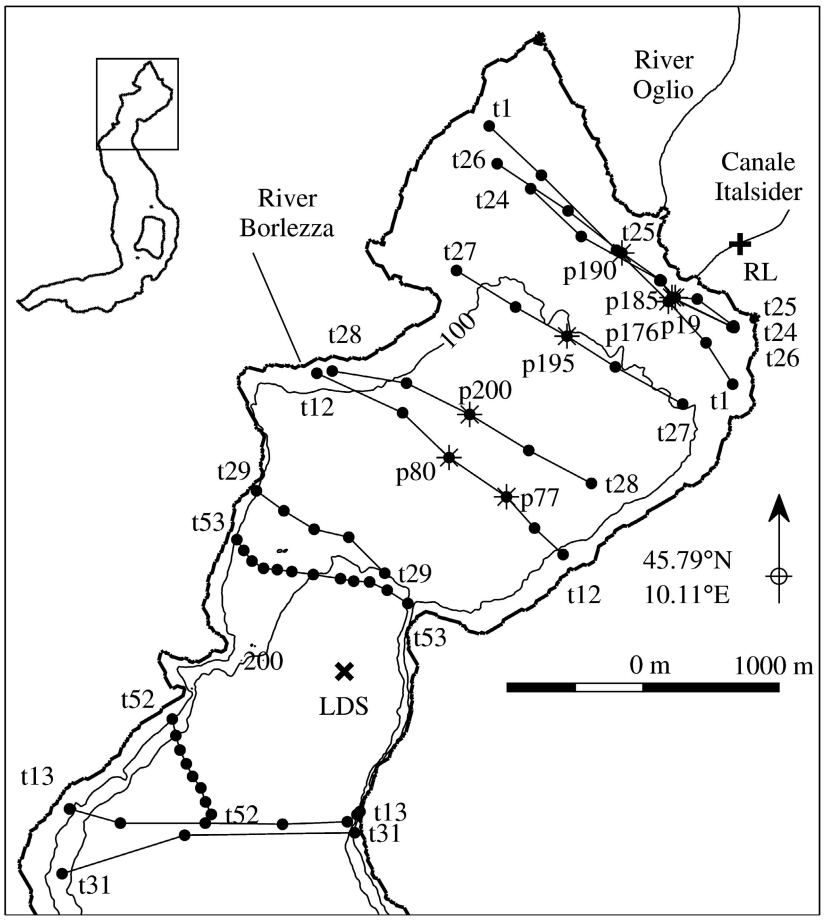

Fig. 5. Map of Lake Iseo's bathymetry. Location of the LDS is shown by × and the river logger by a cross. The Oglio River logger was located 10 km upstream from the lake, outside the frame. Profile stations are marked by filled circles apart from Sta. p19, p77, p80, p176, p185, p190, 195, and p200, which are marked by asterisks and identified individually. The transects are indicated with lines and named.

Methods

Field experiment—A multi-objective field campaign was undertaken in Lake Iseo, Italy (45.7°N, 10.0°E), from 14 to 28 July 2010 (ordinal date 195 to 209) (Valerio et al. 2012). We report here only on the data from the field campaign that are relevant to our objective, determining the length scales and mixing in the consecutive stages of the interflow in the northern part of the lake. Lake Iseo, shown in Fig. 5, is a natural, meromictic, eutrophic, freshwater lake situated in the foothills of the Alps. The surface area is 62 km^2, maximum depth 250 m, and volume 7.6 km^3. The lake's geomorphology was reported by Bini et al. (2007). Lake Iseo is oriented along the north–south axis of a steep-sided valley. The main inflows, the Oglio River and the Canale Italsider, enter at the northern shore and would fill the lake in ~ 4 yr (Salmaso et al. 2003). These rivers bring snowmelt and runoff from a series of reservoirs from the catchment north of the lake. Industrial effluents are discharged into the Oglio River and Canale Italsider, which cause daily fluctuations in the salinity of both inflows.

During the field campaign, the temperature at the bottom of the lake was 6.4°C and the peak surface temperature was 26.8°C. The density stratification throughout the lake was dominated by the temperature variations. Salinity had negligible effect on the density of river or lake water discussed in this paper and was effectively a passive tracer. The metalimnion extended between 5 and 30 m. The wind over the lake generally oscillated between northerly katabatic winds at night and southerly anabatic winds in the day, which generated the internal wave field within the basin (Valerio et al. 2012).

During the field campaign, the Oglio River had an average discharge of 9.8 m^3 s^{-1} (standard deviation [SD]: 3.8 m^3 s^{-1}; minimum: 2.3 m^3 s^{-1}; maximum: 22.1 m^3 s^{-1}), average salinity of 0.33 (SD: 0.05; minimum: 0.17; maximum: 0.41), and average temperature of 14.6°C (SD: 1.7°C; minimum: 11.6°C; maximum 19.0°C). Salinity will be reported in units of g kg^{-1} solution throughout this paper. The Canale Italsider is located 500 m east of the Oglio River, as shown in Fig. 5. During the field campaign the Canale Italsider had an average discharge of 40 m^3 s^{-1} (SD: 4.7 m^3 s^{-1}; minimum: 30.5 m^3 s^{-1}; maximum: 48 m^3 s^{-1}), average salinity of 0.13, and average temperature of 13.0°C (SD: 0.7°C; minimum: 11.3°C;

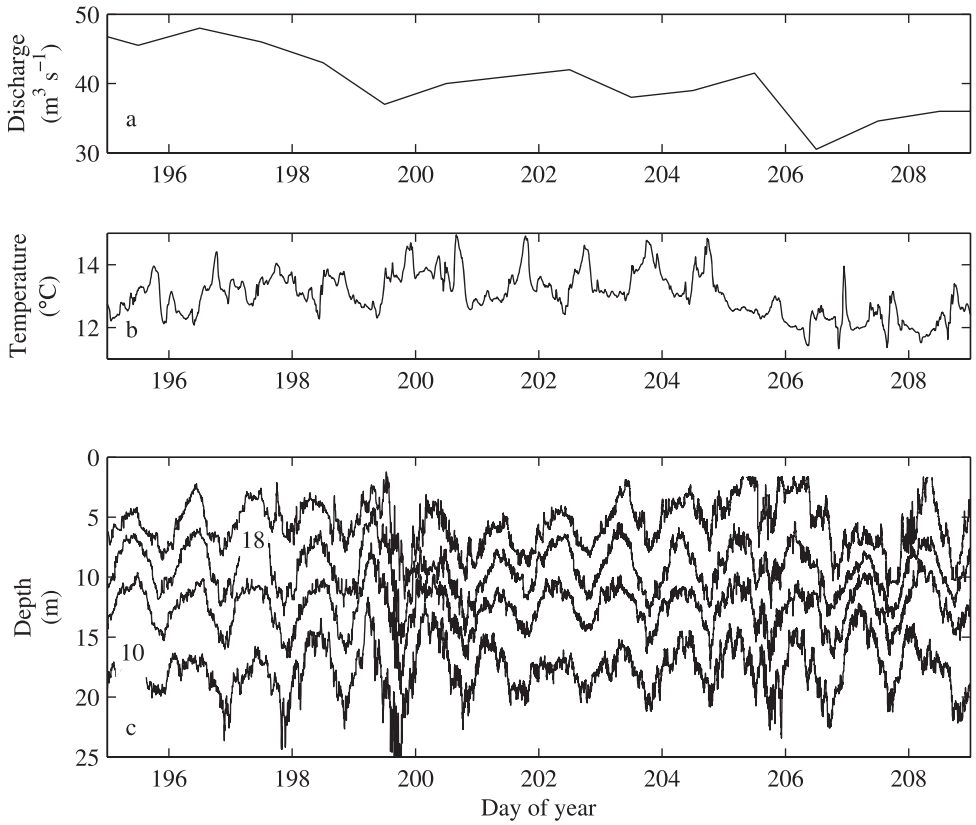

Fig. 6. Time series of (a) discharge and (b) temperature of the Canale Italsider and (c) isotherm depths measured by the thermistor chain.

maximum: 14.9°C). The River Borlezza enters at the northwest of the lake, as shown in Fig. 5, and had a discharge of ~ 2 m^3 s^{-1} and a salinity of 0.44. This river had only a negligible hydrodynamic effect on the lake and provided a minor salinity tracer source. The Canale Italsider dominated the volume flow into the lake during the field campaign. This river had Fr_0 of 2.5 and sharply diverging riverbanks at the inlet to the lake, which suggests that the plunge region should be categorized as case 4, described above.

Instrumentation—The location of instrumentation used in this study is shown in Fig. 5. A Lake Diagnostic System (LDS) deployed in open water in the northern part of the lake consisted of meteorological sensors (wind speed and direction, net total radiation, incoming shortwave radiation, air temperature, and relative humidity) located 2 m above the water surface and a thermistor chain equipped with 21 thermistors measuring the water temperature at different depths that varied from 0.25 to 49.75 m (Imberger 2004). The sensors were sampled at 10 s intervals. River data loggers were installed on the two main inflows, the Oglio River and the Canale Italsider, sampling at 5 min intervals. The logger in the Oglio River was located at a weir upstream of the lake and measured water level, temperature, and conductivity. The inflow rates were estimated by applying the weir rating curve to the measured water level. The logger in the Canale Italsider measured temperature. The daily inflow rates were taken from the hydropower plant that controls the flow to the Canale Italsider. The conductivity within the Canale Italsider was

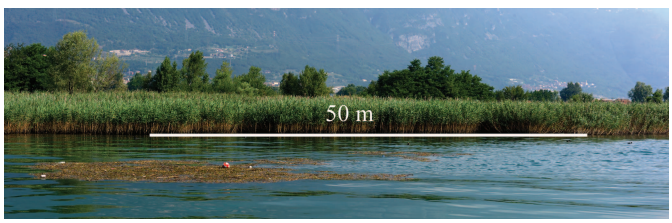

Fig. 7. Photograph showing the size of the plunge region and the buildup of flotsam that identified the extent of the plunge region. The scale indicates 50 m along the bank of the river.

Table 1. Characteristics of the inflow used in calculating the plunge region length scale.

Parameter	Value
Inflow channel width (m)	49
Inflow channel depth (m)	1.7
Inflow velocity (m s^{-1})	0.48
Inflow reduced gravity (m s^{-2})	0.021
Inflow temperature (°C)	13.0
Lake surface temperature (°C)	24.2
Inflow density (kg m^{-3})	999.4
Lake surface density (kg m^{-3})	997.3

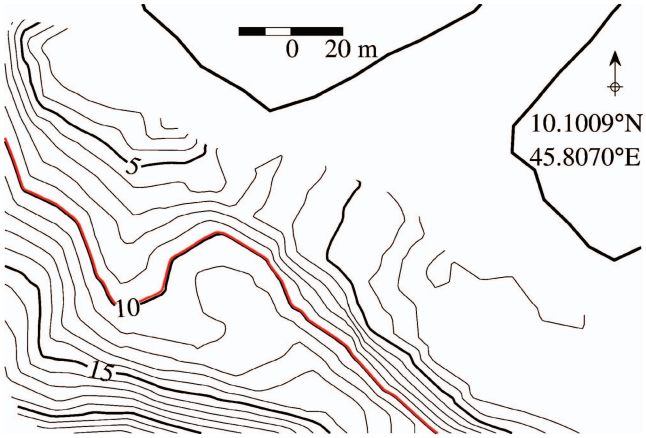

Fig. 8. Bathymetry in the neighborhood of the Canale Italsider inlet. The isobath of the neutral buoyancy level predicted by the numerical underflow model is given by the red line.

measured on three occasions during the field experiment. Temperature and conductivity measurements taken after the field campaign at 3 min intervals between 01 and 24 June 2011 found the mean salinity to be 0.08. This supports the measurements taken during the field campaign, to within the expected interannual variability, showing that the Canale Italsider was lower in salinity than the Oglio River. The inflow conditions of the Canale Italsider and the thermal structure of the lake measured at the LDS are shown in Fig. 6.

The Multi-scale Profiler (MSP) comprises: a C6 Multi-Sensor Platform™ submersible fluorometer with six Cyclops-7™ fluorescence and turbidity sensors and the device's standard temperature and pressure sensors; a fine-scale probe (Imberger and Head 1994) measuring pressure, temperature (with accuracy better than 0.001°C), conductivity (with accuracy better than 0.001 S m^{-1}), dissolved oxygen (DO) (with accuracy better than 0.1 mg L^{-1}), pH, and photosynthetic active radiation; and a microstructure probe with pressure and fast temperature sensors. The MSP is a free-fall profiler, falling at about 0.15 m s^{-1}. The fine-scale sensors were sampled at 50 Hz, the microstructure at 100 Hz, and the C6 at 1 Hz. Rhodamine WT, chlorophyll *a* (Chl *a*), colored fraction of dissolved organic matter (CDOM), and turbidity sensors were installed on the C6 unit. The fine-scale sensor signals were digitally enhanced, as described by Fozdar et al. (1985), in order to match the sensor responses and avoid spiking in the quantities derived from multiple signals, e.g., salinity. The Chl *a* fluorescence measurements were calibrated against laboratory determinations of Chl *a* in water samples taken alongside profiles at eight stations spanning the lake. Opportunistic MSP profiling was conducted over several days along longitudinal and cross transects taken throughout the lake.

Table 2. Parameter values used in calculating underflow length scale for Canale Italsider.

Parameter	Value
Inflow temperature (°C)	13.0
Volume flow rate (m^3 s^{-1})	40
Bottom drag coefficient (C_D)	0.016
Average bed slope angle (°)	4.6
Valley half angle (°)	86

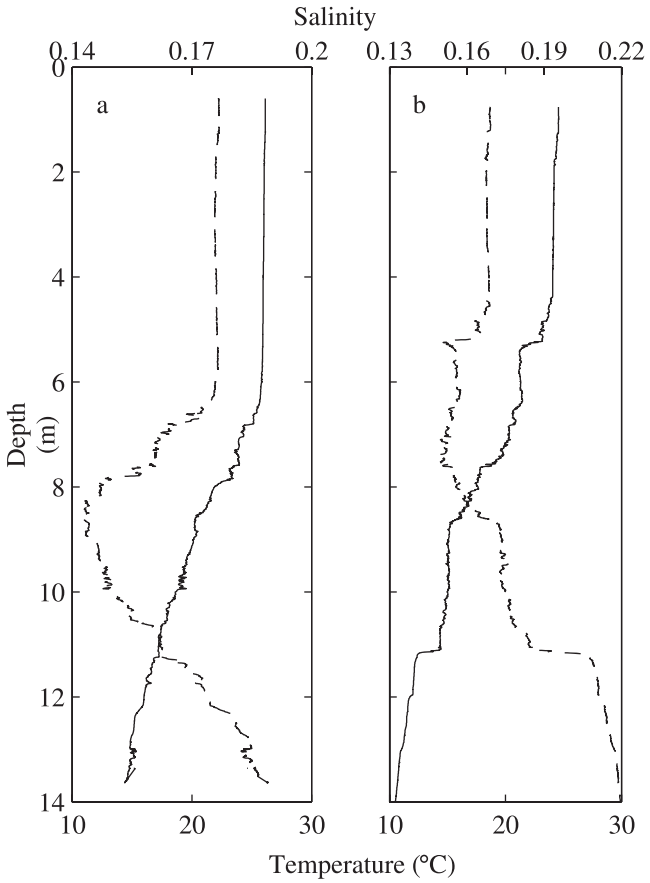

Fig. 9. Profiles of salinity (dashed line) and temperature (solid line) at Sta. (a) p19 and (b) p185.

The small differences in salinity between the river and lake waters allowed the dilution rate of the inflow to be calculated. The small salinity differences require an accurate method of calculating the salinity to achieve accurate dilution rate calculations. The relationship between the measured conductivity and salinity of water depends on the species of ions present in the water. The ionic species can be taken into account by using the method described by Pawlowicz (2008). The ionic content of water in Lake Iseo was 2.19 meq L^{-1} calcium, 1.89 meq L^{-1} bicarbonate, 0.67 meq L^{-1} magnesium, and 1.04 meq L^{-1} sulfate (Ambrosetti and Barbanti 2005). This ratio of ions was used to calculate salinity of all water in the lake because all the water comes from the same catchment.

The dissipation of TKE was determined by analysis of the temperature microstructure profiles as described in Luketina and Imberger (2001). Briefly, after filtering to correct for response time (Fozdar et al. 1985), the profiles were partitioned into statistically stationary segments (Imberger and Boashash 1986; Imberger and Ivey 1991; Luketina and Imberger 2001). The temperature gradient signal from each stationary signal was then analyzed

Table 3. Measured mixing ratios (γ_u) for intrusions based on natural tracers.

Profile station	Salinity	Temperature	DO	CDOM	Turbidity	Average of all estimates
p19	0.8	1.6	1.3	0.6	0.4	1.0
p185	2.0	1.5	0.6	1.2	4.0	1.9

using a Batchelor curve fitting technique to evaluate the dissipation of TKE, ϵ. The upper bound of the vertical mixing coefficient was evaluated from the Osborn (1980) formula (Yeates et al. in press):

$$\kappa = 0.2\frac{\epsilon}{N^2} \tag{14}$$

Results

Plunge region—The plunge curve, formed by the water issuing from the Canale Italsider, was identified visually in the field by the buildup of flotsam at the convergence zone, about 30 to 50 m from the separation point, as shown in Fig. 7; the separation point was located at the start of the increase in the width of the river. The inflow characteristics measured during the field campaign are given in Table 1. The river velocity was found by dividing the average volume flow rate during the campaign by the channel cross-sectional area. The reduced gravity was calculated from the difference between the average temperature of the river during the experiment and the average temperature at the 0.25 m deep thermistor at the LDS during the experiment. The average entrance Froude number Fr_0 was 2.5 and indicated that lateral collapse (case 4) was the relevant plunging mechanism. The model for lateral collapse, Eq. 12, gave a distance to the plunge region vertex of 120 m, in reasonable agreement with the plunge curve visible in Fig. 7. The laboratory measurements show the mixing ratio in a plunge region undergoing lateral falling has a constant value of 0.06 (Britter and Simpson 1978).

Underflow—The entrainment during the underflow and the depth at which the underflow lifts away from the lake bed were calculated using the assumption of gradually varied flow from Eq. 4 (Antenucci et al. 2005). The lake stratification, inflow temperature, and volume flow rate were averaged over the duration of the experiment. The bathymetry around the river mouth was available from an echo sounder survey of the lake with a nominal horizontal resolution of 10 m (Bini et al. 2007). The river channel was assumed to have a triangular cross section with a bottom drag coefficient typical for a sandy bed (Fischer et al. 1979). The bed slope was averaged over the first 100 m of the thalweg from the inlet. The base angle of the triangular cross section of the river channel was found by averaging five cross sections over the first 50 m from the river mouth. The bathymetry around the Canale Italsider inlet is shown in Fig. 8. Using the values given in Table 2, the calculation of the underflow behavior gives a neutral buoyancy depth of 9.9 m, corresponding to the 18°C isotherm, and a mixing ratio of 1.1. The bathymetry reaches this depth at a distance of the order of 100 m offshore from the inlet.

Measurement of underflow dilution—The mixing ratio during the underflow (γ_u) was calculated from the changes in concentration of conserved quantities between the upstream river and the beginning of the intrusion. The quantities used—salinity, temperature, DO, CDOM, and turbidity—were naturally present in the water and assumed to be conservative over the time taken for the water to pass through the underflow; DO, CDOM, and turbidity are quasi-conservative over the time taken for the water to pass through the underflow, so they gave additional estimates of the mixing ratio, although less accurate than those obtained from salinity and temperature.

The underflow mixing ratio was calculated using

$$\gamma_u = \frac{c_r - c_i}{c_i - c_s} \tag{15}$$

where c_r is the concentration of a conserved quantity in the river water, c_s the average concentration in the lake surface water, and c_i the concentration in the intrusion. The river concentrations were measured in the river upstream of the plunge region, so the estimate of underflow mixing ratio includes the contribution of the plunge region mixing. The plunge region mixing caused by the lateral falling mechanism was, however, small relative to the underflow mixing.

In order to calculate c_i, the intrusion water was identified by the following method. Profiles in the northern basin were selected in which the Canale Italsider intrusion could be identified from anomalies in the salinity measurements. Anomalies that occurred in statically unstable regions were discarded because they were the result of turbulent overturns, not intrusions. The profiles selected were p19 and p185; the locations of these stations are shown in Fig. 5 and the profiles of salinity and temperature are shown in Fig. 9. The upper and lower extents of the intrusion were demarcated by sharp salinity and temperature changes bounding the intrusion. Such changes are apparent in Fig. 9 at depths of 6.8 m, 7.5 m, 10.6 m, and 11.2 m in p19 and 5.3 m, 8.6 m, and 11.1 m in p185. To choose between the alternative upper and lower extents present in the profile, the extents selected were those that were most self-consistent (i.e., led to the least variance between mixing ratios estimated from the different tracers). The calculated mixing ratios are shown in Table 3. The average γ_u over both underflows was 1.5. The mixing rates measured in the two intrusions based on the strictly conserved quantities of temperature and salinity ranged from 0.8 to 2.0.

Intrusion—Intrusion waters from both the Oglio River and Canale Italsider were clearly apparent in the salinity,

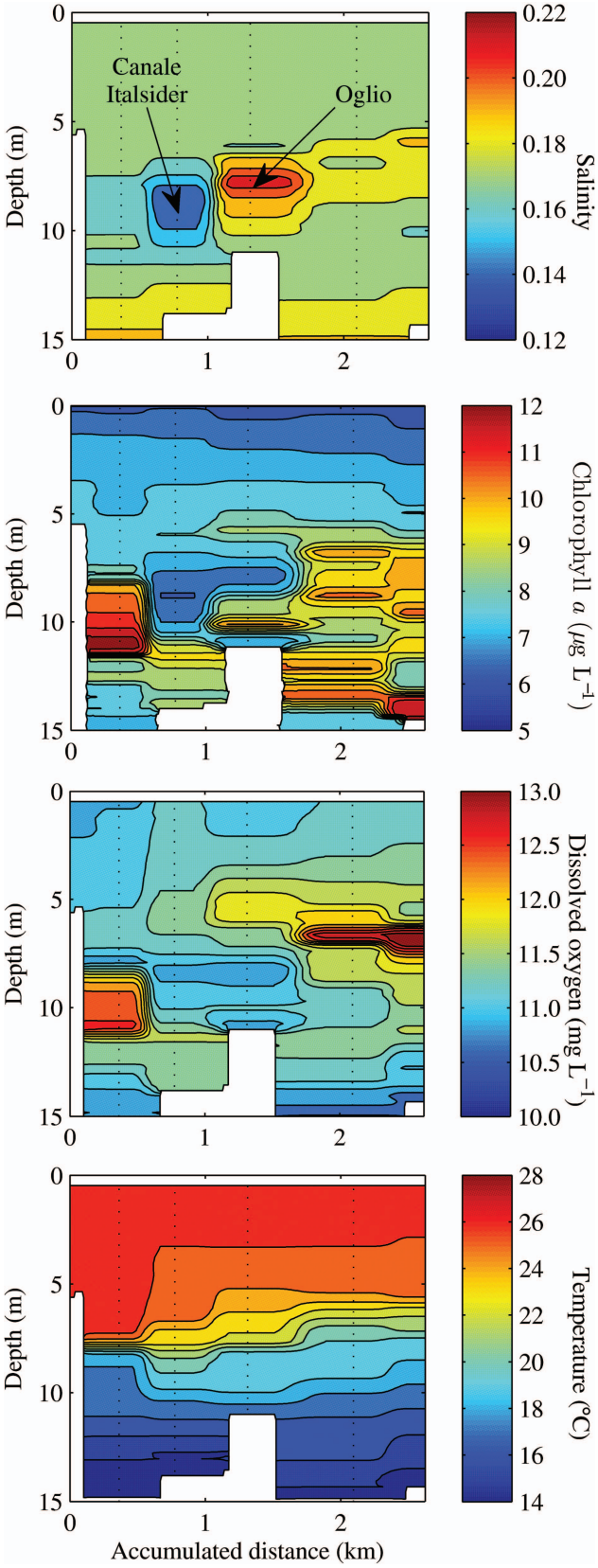

Fig. 10. Transverse transect of salinity, Chl *a* concentration, DO concentration, and temperature at transect t1, as viewed looking downstream. The profiles were taken between 17:06 h and 18:14 h on day 196. The plots show the fresher water intruding from the Canale Italsider and the saltier water intruding from the River Oglio. Reduced Chl *a* and DO concentrations and reduced temperature stratification of the intrusions are apparent at the same positions. The location of the profiles are indicated with dotted lines. Values were interpolated with a finite impulse response filter between profiles.

DO, and Chl *a* fields of the transverse transect t1 taken 300 m from the shore, as shown in Fig. 10. The fresher water of the Canale Italsider intrusion can be seen 0.5 km along the transect and the saltier water of the Oglio intrusion can be seen 1.5 km along the transect. The inflows both had Chl *a* concentrations of 0.8 μg L^{-1}, significantly lower than the lake water. The Oglio River and Canale Italsider inflows had DO concentrations of 10.0 and 10.8 mg L^{-1}, respectively, again significantly lower than the lake water. The regions of anomalies in the Chl *a* and DO were collocated with each other and the salinity anomalies. At the same location, the isotherms, shown in Fig. 10, are spread apart by the intrusions which introduce water with a more uniform density than water at this depth in the lake. The collocation of the anomalies in all the different measured quantities supports the hypothesis that these two regions are intrusions consisting of water from the inlets. In transects further from the inlets than transect t1, the intrusion waters were harder to identify because the anomalies caused by the intrusions were weaker.

General salinity pattern in the northern basin—The salinity measurements at transect t1 show that both the surface and deep water were saltier than the intrusion from the Canale Italsider. Throughout the northern basin the water around the 20°C isotherm typically possessed a minimum in salinity, as shown in profile p176 in Fig. 11. This may be explained by noting that the Oglio River inflow was more buoyant than the Canale Italsider. The Oglio River intrusion therefore entered the lake slightly above the Canale Italsider. The surface mixed layer was therefore slightly saltier as it contained a larger proportion of the Oglio River water. The water around the 20°C isotherm contained the highest concentration of fresh Canale Italsider water, causing the minimum in salt content. At depths below the Canale Italsider intrusion, the proportion of the water retained from the previous winter increased. Water retained from the previous winter was saltier than the Canale Italsider intrusion because the upper part of the lake mixes during the winter, attaining a salinity between those of the Oglio River and Canale Italsider (Mosello et al. 2010).

The horizontal extent of the relatively undiluted intrusion water from the two inflows is apparent in the horizontal section of salinity, averaged between the 18°C and 22°C isotherms, shown in Fig. 12. The values of the upper and lower bounding isotherms were selected to encompass the depths at which the salinity signals of the intrusions were observed most strongly. The resulting salinity distributions were found to be insensitive to the exact values of these bounds. The inflow from the Canale

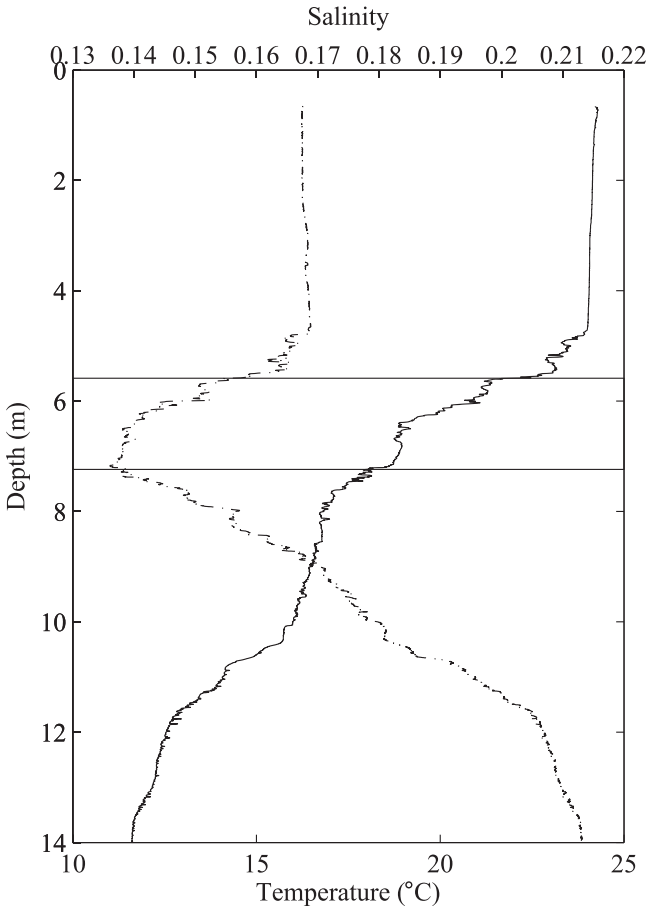

Fig. 11. Profiles of salinity (dot-dashed) and temperature (solid) at p176 taken on day 202. The representative bounds of the intrusion in the northern basin, between the 18°C and 22°C isotherms, are indicated by the dashed lines.

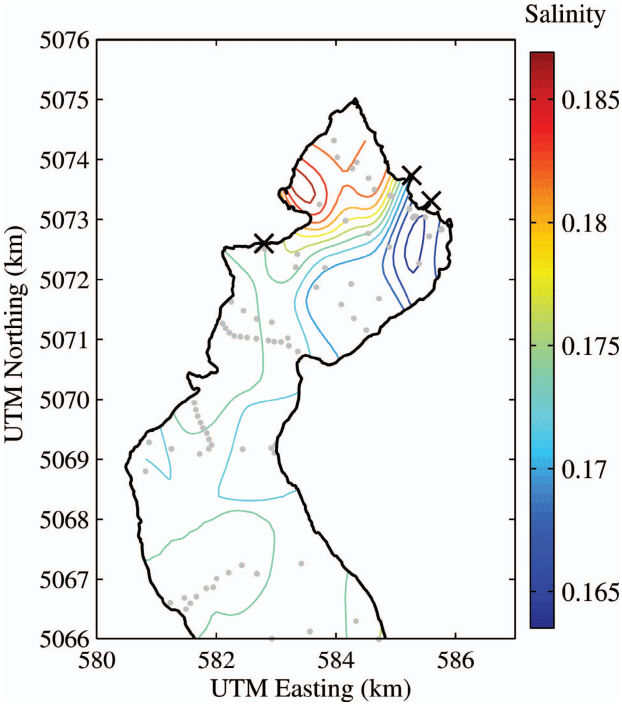

Fig. 12. Horizontal cross section of salinity at the isotherm of the Canale Italsider intrusion. The locations of the profiles are indicated by dots. Values were interpolated with a finite impulse response filter. Inflow locations are marked by ×. The axes give the Universal Transverse Mercator (UTM) coordinates.

Italsider may be considered steady over the time taken for the water to travel the length of the intrusion, as shown in Fig. 6. Within approximately 5 km of the inlets, the western part of the lake was dominated by higher salinity water and the eastern part of the lake was dominated by lower salinity water coming from the Canale Italsider. Further than 5 km from the inlets, the lake water at the depth of the intrusion became relatively homogenous.

Intrusion dynamics—Calculation of the length scales of the intrusion from dynamical considerations requires measurement of the vertical turbulent diffusivity at the depth of the intrusions. The locations of the microstructure profiles used (p19, p77, p80, p176, p185, p190, 195, and p200) are shown in Fig. 5 and the TKE dissipation estimates obtained from temperature gradient profiles are shown in Fig. 13. Within the intrusion region, defined by the 18°C and 22°C isotherms, the TKE dissipation varied between 6×10^{-9} m^2 s^{-3} and 7×10^{-7} m^2 s^{-3} with an average value in this region of 1.1×10^{-7} m^2 s^{-3}. Such variation may be expected as each profile records one event at a particular time (Imberger and Ivey 1991). The average buoyancy frequency in the region of the intrusion was 0.046 s^{-1}, yielding an average vertical turbulent diffusivity, from Eq. 14, of 1.0×10^{-5} m^2 s^{-1}. The thickness of the inertia-buoyancy intrusion was calculated, from the equation for a 2D intrusion, Eq. 7, to be 0.9 m. The 2D volume flux was calculated from the combined river inflow and entrained fluid volume flux, 74 m^3 s^{-1}, and the width of the lake, 2100 m. The horizontal length scale over which the intrusion was governed by an inertia-buoyancy force balance, calculated using Eq. 5 with the values given in Table 4, was 3 km. The horizontal length scale for diffusion to reduce the concentration of the inflow tracer in the diffusive-buoyancy regime, calculated using Eq. 11 with the values given in Table 5, was 900 m. These measurements yield a total length scale of 4 km (3.9 km) for the inflow intrusion to be integrated into the lake water, in good agreement with that observed from the salinity in Fig. 12. The estimated length scales of the consecutive stages of the Canale Italsider interflow, which are calculated above, are summarized in Table 6.

Discussion

The amount of mixing and length scales observed for the stages of the Canale Italsider interflow will now be compared to the results of previous studies and the implications for lake models will be highlighted.

Inflow mixing—In their previous study, Spigel et al. (2005) observed a value of γ_p of 1.9 in the plunge region of both rivers, which is much larger than the value of 0.06 predicted by the laboratory experiments of Britter and

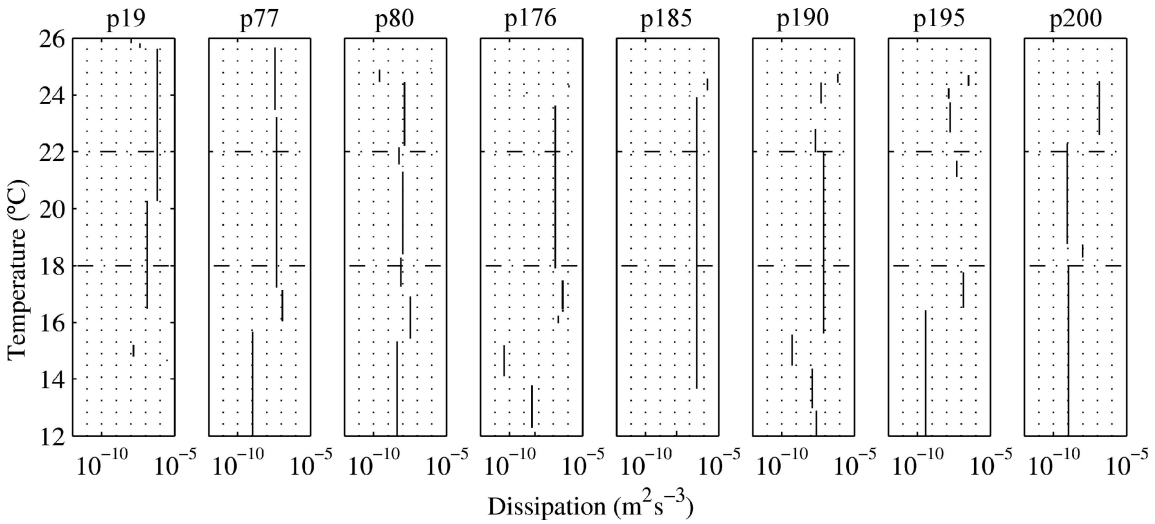

Fig. 13. Profiles of dissipation plotted with temperature at Sta. p19, p77, p80, p176, p185, p190, 195, and p200. The representative bounds of the intrusion in the northern basin, the 18°C and 22°C isotherms, are indicated by the dashed lines.

Simpson (1978). The larger γ_p was caused by the inflows being in the entraining jet regime for larger Fr_0. The values of Fr_0 reported by Spigel et al. (2005), 2.6 in the Tongariro River and 3.4 in the Tokaanu Tailrace, were underestimated because these reported values were based on a length scale formed from the square root of the cross-sectional area rather than the water depth. To illustrate this, the river depth at the mouth of the Tokaanu Tailrace, while not reported specifically at the separation point, was 1.4 m, which gives a much larger Fr_0 of 69. At this large value of Fr_0, the higher values of γ_p observed are as expected from a laterally entraining jet. In the series of experiments by Johnson et al. (1987), six runs were carried out in channels that immediately widened upon meeting the lake and in which $Fr_0 < 3$. Of these runs, five runs used channels with aspect ratio $W:H$ of 0.5 and these had values of γ_p ranging from 2.1 to 3.5. In the other relevant experimental run, $W:H$ was 2 and γ_p was 0.5. These entrainment rates are higher than those predicted by Britter and Simpson's (1978) experimental results because $W:H$ is of order unity rather than being much larger than unity. In channels with deep, narrow inflows, the relatively large lateral surface area of the inflow allows horizontal entrainment to be significant, shown by the trend of reduced γ_p with increased $W:H$ in the results of Johnson et al. (1989). The vertical entrainment that occurs as the river water falls below the lake water, measured by Britter and Simpson's experiments (1978), is not dominant in channels with these small aspect ratios. In typical river inlet geometries, as in the Canale Italsider inlet to Lake Iseo, the aspect ratio $W:H$ is much larger than unity, which means that the entrainment predominantly occurs as river water falls beneath the lake water and the experimental results of Britter and Simpson (1978) are applicable. The value of γ_p reported by Rueda and MacIntyre (2009) is 0.7 for an inlet with $Fr_0 = 2.8$. This value of γ_p, while smaller than values reported elsewhere, is not as small as the value predicted by the experiments of Britter and Simpson (1978). We suspect this is because Fr_0 is not small enough.

The results in the prior literature, along with those reported here, suggest that the linear relationship between Fr_0 and γ_p in Eq. 3 is not appropriate over the entire range $1 < Fr_0$. The experimental results of Britter and Simpson (1978), expressed in Eq. 13, provide a suitable estimate in the regime of Fr_0 slightly larger than unity. Improved parameterizations of γ_p, which are applicable to all plunging inflows that meet the geometric criteria, should allow for different regimes at small and large Fr_0. These two regimes correspond to the lateral falling and entraining jet mechanisms.

The dilution of conserved quantities calculated from field observations indicates a total mixing ratio of 1.5. The numerical entrainment calculated using the method described by Antenucci et al. (2005) agrees with the measured mixing ratio to within the level of variability present between estimations from different tracers. The calculations of mixing ratios in the plunge region and underflow show that the majority of entrainment into the Canale Italsider interflow occurs in the underflow, with a ratio $\gamma_p:\gamma_u$ of 0.04. For a model to describe the Canale Italsider

Table 4. Field measurements used in calculating the horizontal length scale of the inertia-buoyancy intrusion.

Parameter	Value
Source volume flow rate per unit width ($m^2\ s^{-1}$)	0.035
Buoyancy frequency (s^{-1})	0.046
Turbulent diffusivity ($m^2\ s^{-1}$)	1.0×10^{-5}

Table 5. Values used to calculate the length scale over which the diffusive-buoyancy intrusion is diluted.

Parameter	Value
Background buoyancy frequency (s^{-1})	0.046
Intrusion thickness (m)	0.9
Turbulent diffusivity ($m^2\ s^{-1}$)	1.0×10^{-5}

Table 6. Summary of the length scales of the consecutive stages of the Canale Italsider interflow.

Length scale	Estimate for Canale Italsider (m)
Offshore extent of plunge curve	120
Horizontal length scale of underflow from the inlet	100
Horizontal length of inertia-buoyancy intrusion	3000
Horizontal length of diffusion-buoyancy intrusion	900

intrusion accurately, the underflow entrainment must be modeled accurately but the plunge region mixing can be neglected. Further tracer-dilution field and laboratory experiments with higher spatial resolution could give separate estimates of the mixing in the plunge region and underflow to further validate these calculations.

The dominance of mixing in the underflow observed in Lake Iseo does not necessarily occur at inlets with other parameter values. When $Fr \gg 1$ or when the bathymetry at the inlet is stepped, the plunge region mixing ratio will be greater (Spigel et al. 2005). When the neutral buoyancy depth in the ambient is reduced, the entrainment into the underflow will reduce because the underflow will not travel as far before lifting away from the lake bed. All mixing processes that contribute substantially to dilution of a specific inflow must be represented accurately in a hydrodynamic model if it is to form a sound basis for pollutant transport or ecological analysis (Botelho and Imberger 2007; Rueda et al. 2007; Vilhena et al. 2010). Models of plunge region mixing are currently lacking and need to be further improved and validated (Dallimore et al. 2004; Rueda and MacIntyre 2010). The application, developed here, of Britter and Simpson's (1978) laboratory results to the plunge region gives a widely applicable improved plunge region mixing model in the regime of Fr_0 slightly larger than unity that can be incorporated into hydrodynamic models of lakes.

Inflow length scales—The length scale of the plunge region observed in the field study supported the lateral falling mechanism. This suggests that the proposed lateral falling mechanism governs how hypopycnal river inflows with sharply diverging riverbanks plunge in the limit of Fr_0 slightly larger than unity. These criteria for lateral falling are met in many river–lake systems in various climates, for at least part of the year (Imberger and Patterson 1989). In any such system, the size of the plunge region can be modeled using Eq. 12 and the amount by which the river water is diluted using Eq. 13. When rivers enter coastal oceans or fjords in geometries similar to that considered in this study, it is reasonable to speculate that, in the absence of other dominating mechanisms such as tidally induced flows, the liftoff of the buoyant inflow from the riverbed will be governed by the same lateral falling dynamics as in the plunging region (Luketina and Imberger 1987).

The intrusion depth calculated by the numerical model of Antenucci et al. (2005), that implies the length scale of the underflow, fell within the range of intrusion depths observed in this field study. The horizontal length scale of the intrusion was of the order of 4 km, supported by both the salinity measurements and calculations based on the intrusion dynamics. This length scale is important from a biological perspective because it is the length scale over which the inflow potential energy transports nutrients; beyond this distance, horizontal dispersion is required to transport the nutrients into the lake.

Acknowledgments

We thank the Centre for Water Research field staff, Marco Pilotti, Giulia Valerio, and Barbara Leoni for assistance with field measurements and the preparation of this paper. We thank Paul Linden, Stuart Dalziel, Peisheng Huang, and Sarah Laborde for helpful discussions during the preparation of this paper. We also thank two anonymous reviewers for their insightful comments. This project was supported by the Australian Research Council Discovery Project DP1096728. The work of C.A.R.H. was supported by the Natural Environment Research Council and Arup, and the work of H.E.H. is supported by the Royal Society Wolfson Research Merit Award. This article constitutes Centre for Water Research reference 2362-CH.

References

Alavian, V., G. H. Jirka, R. A. Denton, M. C. Johnson, and H. G. Stefan. 1992. Density currents entering lakes and reservoirs. J. Hydraul. Eng. **118:** 1686–1691, doi:10.1061/(ASCE)0733-9429(1992)118:12(1686)

Ambrosetti, W., and L. Barbanti. 2005. Evolution towards meromixis of Lake Iseo (Northern Italy) as revealed by its stability trend. J. Limnol. **64:** 1–11, doi:10.4081/jlimnol.2005.1

Antenucci, J. P., J. D. Brookes, and M. R. Hipsey. 2005. A simple model for quantifying *Cryptosporidium* transport, dilution and potential risk. J. Am. Water Works Assoc. **97:** 86–93.

Benjamin, T. B. 1968. Gravity currents and related phenomena. J. Fluid Mech. **31:** 209–248, doi:10.1017/S0022112068000133

Bini, A., D. Corbari, P. Falletti, M. Fassina, C. R. Perotti, and A. Piccin. 2007. Morphology and geological setting of Iseo Lake (Lombardy) through multibeam bathymetry and high-resolution seismic profiles. Swiss J. Geosci. **100:** 23–40, doi:10.1007/s00015-007-1204-6

Botelho, D. A., and J. Imberger. 2007. Dissolved oxygen response to wind-inflow interactions in a stratified reservoir. Limnol. Oceanogr. **52:** 2027–2052, doi:10.4319/lo.2007.52.5.2027

Britter, R. E., and J. E. Simpson. 1978. Experiments on the dynamics of a gravity current head. J. Fluid Mech. **88:** 223–240, doi:10.1017/S0022112078002074

Cáceres, M., A. Valle-Levinson, H. H. Sepúlveda, and K. Holderied. 2002. Transverse variability of flow and density in a Chilean fjord. Cont. Shelf Res. **22:** 1683–1698, doi:10.1016/S0278-4343(02)00032-8

Chen, J. C. 1980. Studies of gravitational spreading currents. Ph.D. thesis. California Institute of Technology.

Dallimore, C. J., J. Imberger, and B. R. Hodges. 2004. Modeling a plunging underflow. J. Hydraul. Eng. **130:** 1068–1076, doi:10.1061/(ASCE)0733-9429(2004)130:11(1068)

———, ———, and T. Ishikawa. 2001. Entrainment and turbulence in saline underflow in Lake Ogawara. J. Hydraul. Eng. **127:** 937–948, doi:10.1061/(ASCE)0733-9429(2001)127:11(937)

Elder, R. A., and W. O. Wunderlich. 1972. Inflow density currents in TVA reservoirs, p. 220–236. *In* Proceedings of the International Symposium on Stratified Flows. IAHR.

Ellison, T. H., and J. S. Turner. 1959. Turbulent entrainment in stratified flows. J. Fluid Mech. **6:** 423–448, doi:10.1017/S0022112059000738

Fernandez, R. L., and J. Imberger. 2006. Bed roughness induced entrainment in a high Richardson number underflow. J. Hydraul. Res. **44:** 725–738, doi:10.1080/00221686.2006.9521724

Fischer, H. B., E. J. List, R. C. Y. Koh, J. Imberger, and N. H. Brooks. 1979. Mixing in inland and coastal waters. Academic Press.

Fleenor, W. E. 2001. Effects and control of plunging inflows on reservoir hydrodynamics and downstream releases. Ph.D. thesis. University of California, Davis.

Ford, D. E., and M. C. Johnson. 1983. An assessment of reservoir density currents and inflow processes. Technical Report E-83-7. Ford, Thornton, Norton, and Associates, Ltd., and the Environmental Laboratory, Waterways Experiment Station, for the U.S. Army Engineer Waterways Experiment Station, Vicksburg, MS.

Fozdar, F. M., G. J. Parker, and J. Imberger. 1985. Matching temperature and conductivity sensor response characteristics. J. Phys. Oceanogr. **15:** 1557–1569, doi:10.1175/1520-0485(1985)015<1557:MTACSR>2.0.CO;2

Hebbert, B., J. Imberger, and I. Loh. 1979. Collie River underflow into the Wellington Reservoir. J. Hydraul. Div., Am. Soc. Civ. Eng. **105:** 533–545.

Hodges, B. R., J. Imberger, A. Saggio, and K. B. Winters. 2000. Modeling basin-scale internal waves in a stratified lake. Limnol. Oceanogr. **45:** 1603–1620, doi:10.4319/lo.2000.45.7.1603

Huppert, H. E., and J. E. Simpson. 1980. The slumping of gravity currents. J. Fluid Mech. **99:** 785–799, doi:10.1017/S0022112080000894

Imberger, J. 1972. Two-dimensional sink flow of a stratified fluid contained in a duct. J. Fluid Mech. **53:** 329–349, doi:10.1017/S0022112072000187

———. 1985. Thermal characteristics of standing waters: An illustration of dynamic processes. Hydrobiologia **125:** 7–29, doi:10.1007/BF00045923

———. 2004. A lake diagnostic system for managing lakes and reservoirs. Water Resour. Impact **6:** 7–10.

Imberger, J, and B. Boashash. 1986. Application of the Wigner–Ville distribution to temperature gradient microstructure: A new technique to study small-scale variations. J. Phys. Oceanogr. **16:** 1997–2012, doi:10.1175/1520-0485(1986)016<1997:AOTWDT>2.0.CO;2

Imberger, J., and R. Head. 1994. Measurement of turbulent properties in a natural system, p. 1–20. *In* C. A. Pugh [ed.], Proceedings of the Symposium on Fundamentals and Advancement in Hydraulic Measurements and Experimentation. ASCE.

———, and G. N. Ivey. 1991. On the nature of turbulence in a stratified fluid. Part II: Application to lakes. J. Phys. Oceanogr. **21:** 659–680, doi:10.1175/1520-0485(1991)021<0659:OTNOTI>2.0.CO;2

———, and J. C. Patterson. 1989. Physical limnology, p. 303–475. *In* J. W. Hutchinson and T. Y. Wu [eds.], Advances in applied mechanics. Elsevier.

———, R. Thompson, and C. Fandry. 1976. Selective withdrawal from a finite rectangular tank. J. Fluid Mech. **78:** 489–512, doi:10.1017/S0022112076002577

Johnson, T. R., C. R. Ellis, and H. G. Stefan. 1989. Negatively buoyant flow in a diverging channel. IV: Entrainment and dilution. J. Hydraul. Eng. **115:** 437–456, doi:10.1061/(ASCE)0733-9429(1989)115:4(437)

———, G. J. Farrell, C. R. Ellis, and H. G. Stefan. 1987. Negatively buoyant flow in a diverging channel. I: Flow regimes. J. Hydraul. Eng. **113:** 716–730, doi:10.1061/(ASCE)0733-9429(1987)113:6(716)

Koh, R. C. Y. 1966. Viscous stratified flow towards a sink. J. Fluid Mech. **24:** 555–575, doi:10.1017/S002211206600082X

Luketina, D. A., and J. Imberger. 1987. Characteristics of a surface buoyant jet. J. Geophys. Res. **92:** 5435–5447, doi:10.1029/JC092iC05p05435

———, and ———. 2001. Determining turbulent kinetic energy dissipation from Batchelor curve fitting. J. Atmos. Oceanic Technol. **18:** 100–113, doi:10.1175/1520-0426(2001)018<0100:DTKEDF>2.0.CO;2

Manins, P. C. 1976. Intrusion into a stratified fluid. J. Fluid Mech. **74:** 547–560, doi:10.1017/S0022112076001948

Marti, C. L., R. Mills, and J. Imberger. 2011. Pathways of multiple inflows into a stratified reservoir: Thomson Reservoir, Australia. Adv. Water Resour. **34:** 551–561, doi:10.1016/j.advwatres.2011.01.003

Morton, B. R., G. I. Taylor, and J. S. Turner. 1956. Turbulent gravitational convection from maintained and instantaneous sources. Proc. R. Soc. London, Ser. A **234:** 1–23, doi:10.1098/rspa.1956.0011

Mosello, R., and others. 2010. Evoluzione recente della qualità delle acque dei laghi profondi dfssudalpini (Maggiore, Lugano, Como, Iseo e Garda) in risposta alle pressioni antropiche e alle variazioni climatiche. Biol. Ambientale **24:** 167–177. [Trend of water quality of the deep subalpine lakes in relation to anthropic pressure and climate.]

Osborn, T. R. 1980. Estimates of the local rate of vertical diffusion from dissipation measurements. J. Phys. Oceanogr. **10:** 83–89, doi:10.1175/1520-0485(1980)010<0083:EOTLRO>2.0.CO;2

Pawlowicz, R. 2008. Calculating the conductivity of natural waters. Limnol. Oceanogr.: Methods **6:** 489–501, doi:10.4319/lom.2008.6.489

Rueda, F. J., W. E. Fleenor, and I. de Vicente. 2007. Pathways of river nutrients towards the euphotic zone in a deep-reservoir of small size: Uncertainty analysis. Ecol. Modell. **202:** 345–361, doi:10.1016/j.ecolmodel.2006.11.006

———, and S. MacIntyre. 2009. Flow paths and spatial heterogeneity of stream inflows in a small multibasin lake. Limnol. Oceanogr. **54:** 2041–2057, doi:10.4319/lo.2009.54.6.2041

———, and ———. 2010. Modelling the fate and transport of negatively buoyant storm-river water in small multi-basin lakes. Environ. Model. Software **25:** 146–157, doi:10.1016/j.envsoft.2009.07.002

Salmaso, N., R. Mosello, L. Garibaldi, F. Decet, M. C. Brizzio, and P. Cordella. 2003. Vertical mixing as a determinant of trophic status in deep lakes: A case study from two lakes south of the Alps (Lake Garda and Lake Iseo). J. Limnol. **62:** 33–41.

Serruya, S. 1974. The mixing patterns of the Jordan River in Lake Kinneret. Limnol. Oceanogr. **19:** 175–181, doi:10.4319/lo.1974.19.2.0175

Sherman, F. S., J. Imberger, and G. M. Corcos. 1978. Turbulence and mixing in stably stratified waters. Annu. Rev. Fluid Mech. **10:** 267–288, doi:10.1146/annurev.fl.10.010178.001411

Shin, J. O., S. B. Dalziel, and P. F. Linden. 2004. Gravity currents produced by lock exchange. J. Fluid Mech. **521:** 1–34, doi:10.1017/S002211200400165X

Spigel, R. H., C. Howard-Williams, M. Gibbs, S. Stephens, and B. Waugh. 2005. Field calibration of a formula for entrance mixing of river inflows to lakes: Lake Taupo, North Island, New Zealand. N. Z. J. Mar. Freshwater Res. **39:** 785–802, doi:10.1080/00288330.2005.9517353

Stefan, H. G., and T. R. Johnson. 1989. Negatively buoyant flow in a diverging channel. III: Onset of underflow. J. Hydraul. Eng. **115:** 423–436, doi:10.1061/(ASCE)0733-9429(1989)115:4(423)

Valerio, G., M. Pilotti, C. L. Marti, and J. Imberger. 2012. Influence of bathymetry and wind field on basin-scale internal wave structure in a stratified lake: Lake Iseo, Italy. Limnol. Oceanogr. **57:** 772–786, doi:10.4319/lo.2012.57.3.0772

Vilhena, L. C., I. Hillmer, and J. Imberger. 2010. The role of climate change in the occurrence of algal blooms: Lake Burragorang, Australia. Limnol. Oceanogr. **55:** 1188–1200, doi:10.4319/lo.2010.55.3.1188

Yeates, P., A. Gomez-Giraldo, and J. Imberger. In press. Observed relationships between microstructure patches and the gradient Richardson number in a thermally stratified lake. Environ. Fluid Mech.

Associate editor: James J. Leichter

Received: 23 May 2012
Accepted: 04 November 2012
Amended: 05 December 2012